Published in final edited form as:

Nature. 2014 October 16; 514(7522): 385–388. doi:10.1038/nature13813.

Rb suppresses human cone precursor-derived retinoblastoma tumors

Xiaoliang L. Xu[1,7], **Hardeep P. Singh**[2,3], **Lu Wang**[1], **Dong-Lai Qi**[2,3], **Bradford K. Poulos**[4], **David H. Abramson**[5], **Suresh C. Jhanwar**[1,6], and **David Cobrinik**[2,3,8,9]

[1]Department of Pathology, Memorial Sloan-Kettering Cancer Center, 1275 York Avenue, New York, NY 10021

[2]The Vision Center, Division of Ophthalmology, Department of Surgery, Children's Hospital Los Angeles, 4650 Sunset Boulevard, Los Angeles, CA 90027

[3]The Saban Research Institute, Children's Hospital Los Angeles, 4650 Sunset Boulevard, Los Angeles, CA 90027

[4]Department of Pathology, Albert Einstein College of Medicine, 1300 Morris Park Avenue, Bronx NY 10461

[5]Ophthalmic Oncology Service, Memorial Sloan-Kettering Cancer Center, 1275 York Avenue, New York, NY 10021

[6]Department of Medicine, Memorial Sloan-Kettering Cancer Center, 1275 York Avenue, New York, NY 10021

[7]Sloan-Kettering Institute for Cancer Research, Memorial Sloan-Kettering Cancer Center, 1275 York Avenue, New York, NY 10021

[8]USC Eye Institute, Department of Ophthalmology, Keck School of Medicine of the University of Southern California, 1450 San Pablo Street, Los Angeles CA 90033

[9]Norris Comprehensive Cancer Center, Keck School of Medicine of the University of Southern California, 1441 Eastlake Avenue, Los Angeles CA 90033

Retinoblastoma is a childhood retinal tumor that initiates in response to biallelic *RB1* inactivation and loss of functional Rb protein. Despite that Rb has diverse tumor suppressor functions and is inactivated in many cancers[1–5], germline *RB1* mutations predispose to

Correspondence and requests for materials should be addressed to: S.C.J. (jhanwars@mskcc.org) and D.C. (dcobrinik@chla.usc.edu).

Supplementary Information is linked to the online version of the paper at www.nature.com/nature.

Author Information SNP array data has been deposited with NCBI GEO under accession number GSE60720.

The authors declare no competing financial interests.

Author Contributions X.L.X., S.C.J., and D.C. designed the study. X.L.X. conducted most of the experiments in S.C.J.'s laboratory supported in part by D.C. H.P.S and D.Q. quantitated Rb knockdown and confirmed effects at different time points. H.P.S. transduced retina with YFP-labeled constructs, and analyzed with X.L.X. L.W. analyzed SNP arrays. D.H.A provided retinoblastoma samples. B.P. provided fetal retina. D.C. wrote the manuscript with assistance from X.L.X. and review by S.C.J.

retinoblastoma far more strongly than to other malignancies[6]. This tropism suggests that retinal cell type-specific circuitry sensitizes to Rb loss, yet the nature of the circuitry and cell type in which it operates have been unclear[7,8]. Here, we show that post-mitotic human cone precursors are uniquely sensitive to Rb depletion. Rb knockdown induced cone precursor proliferation in prospectively isolated populations and in intact retina. Proliferation followed the induction of E2F-regulated genes and depended upon factors having strong expression in maturing cone precursors and crucial roles in retinoblastoma cell proliferation, including MYCN and MDM2. Proliferation of Rb-depleted cones and retinoblastoma cells also depended upon the Rb-related p107, SKP2, and a p27 downregulation associated with cone precursor maturation. Moreover, Rb-depleted cone precursors formed tumors in orthotopic xenografts with histologic features and protein expression typical of human retinoblastoma. These findings provide a compelling molecular rationale for a cone precursor origin of retinoblastoma. More generally, they demonstrate that cell type-specific circuitry can collaborate with an initiating oncogenic mutation to enable tumorigenesis.

RB1-mutant retinoblastomas can originate from a cellular state found during retinal development in humans but not other species[9,10]. Accordingly, to identify the cellular state and corresponding circuitry that sensitizes to *RB1* inactivation, we examined effects of Rb depletion on human fetal retinal cells. Samples were from post-fertilization week (FW) 17–19, when all retinal cell types and a range of maturation states are present.

Dissociated retinal cells were transduced with *RB1*-directed or control short hairpin RNAs (shRNAs), followed by co-staining for the proliferation-associated Ki67 and cell type-specific markers. *RB1* shRNAs abrogated Rb expression in long or medium wavelength (L/M)-opsin^{+} and thyroid hormone receptor β2 (TRβ2)$^{+}$ cone precursors as well as in other cell types (Extended Data Fig. 1a). After two weeks, Ki67 was detected in cone precursor-like cells co-expressing the photoreceptor marker CRX and the cone markers L/M-opsin, cone arrestin, and RXRγ (Fig. 1a, Extended Data Fig. 1b–h). Ki67^{+} cone marker^{+} cells were first detected 9 days after transduction whereas clusters were routinely detected by day 23. Ki67 was not detected in cells expressing markers of rods (NRL), bipolar cells (strong CHX10), ganglion cells (BRN-3), or amacrine or horizontal cells (PROX1^{+} or PAX6^{+}, nestin$^{(-)}$) (Fig. 1a, Extended Data Fig. 1i, j). Ki67 was detected in cells expressing markers of RPCs or Müller glia (nestin or CRALBP, SOX2), yet in similar proportions after sh*RB1* or control shRNA (Fig. 1a, Extended Data Fig. 1j). *RB1* shRNAs also induced incorporation of 5-ethynyl-2′-deoxyuridine (EdU), an indicator of S phase entry, increased expression of the mitosis marker phosphohistone H3, suppressed expression of the apoptosis marker cleaved caspase 3 (CC3), and induced proliferation in cells expressing cone but not other retinal cell markers (Fig. 1c, d; Extended Data Fig. 1k–n). In contrast, *RB1* shRNAs induced CC3 and decreased the number of cells expressing markers of RPCs and glia (Fig. 1b, d; Extended Data Fig. 1n).

To assess whether the Rb-deficient proliferating cone-like cells derived from post-mitotic cone precursors, we examined effects of Rb knockdown in prospectively isolated retinal cell populations. Populations were isolated by sorting for size, for CD133, which is expressed strongly in maturing photoreceptors and weakly in RPCs[11], and for a CD44 epitope expressed by Müller glia and RPCs[12] (Fig. 2a). Staining for cell type-specific markers

revealed populations enriched for cone precursors, for rod plus cone precursors, for RPCs plus glia, and for a mixture of rod, ganglion, bipolar, amacrine, and horizontal cells (Fig. 2b, Extended Data Fig. 2a–g). In medium and large CD133^{hi}, CD44$^{(-)}$ populations, 96–98% of cells co-stained for CRX and cone arrestin, which is cone-specific at FW 19 (Extended Data Fig. 2h). A similar enrichment was observed when cone precursors were identified using CRX and RXRγ (Extended Data Fig. 2h–k).

RB1 shRNAs induced similar *RB1* knockdown in each retinal cell population (Extended Data Fig. 3a). After two weeks, Ki67 was detected in 80% of cells in the cone-enriched population (Fig. 2c), likely reflecting a high ratio of shRNA-expressing lentivirus to target cells and cone precursor proliferation. After three weeks, cone precursor numbers increased (Fig. 2c). Rb depletion did not induce proliferation in RPCs and glia, but increased the proportion of CC3+ cells entering apoptosis (Fig. 2c). Sorted populations transduced with the scrambled control had higher CC3^{+} rates than unsorted cultures, potentially reflecting separation of RPCs and glia from neurons[13,14]. Nevertheless, Rb knockdown induced proliferation and apoptosis in cells with the same immunophenotypes as in unsorted cultures. Notably, Rb depletion induced the cell cycle-related genes *CCNE1*, *SKP2*, *E2F1*, *RBL1*, *CCNB1*, and *CDK1* in cone precursors and induced p53-responsive genes in sorted RPCs and glia (Extended Data Fig. 3). Cell cycle-related genes were induced several days before Ki67, suggesting that further reprogramming was needed for cell cycle entry.

RB1 shRNAs also induced cone precursor proliferation in intact retinas. Ki67 was detected in L/M-opsin^{+} cone precursors in the fovea, demarcated by cones but not rods, 15 days after transduction (Fig. 2d). Ki67 was not detected in cells expressing rod, amacrine, horizontal, or ganglion cell markers (Extended Data Fig. 4a, d). Ki67 was detected in RPCs and glia marked by PAX6^{+}, nestin^{+} or by CHX10^{+}, CRX$^{(-)}$, yet in similar proportions after sh*RB1* and control shRNAs (Extended Data Fig. 4b–d). Moreover, a yellow fluorescent protein (YFP) -expressing sh*RB1* vector selectively induced Ki67 in YFP^{+} cones, although all cell types were transduced (Extended Data Fig. 4e–h).

We next determined whether Rb-depleted cone precursors and retinoblastoma cells depend upon similar signaling circuitry. Retinoblastoma cell proliferation requires several proteins that are prominent in cone precursors, including TRβ2, RXRγ, MYCN, and MDM2[7]. Depletion of these factors suppressed Ki67 expression and cone precursor proliferation both in dissociated retinal cultures (Extended Data Fig. 5a, b) and in isolated populations (Fig. 3a). Retinoblastoma cell proliferation also requires SKP2-mediated degradation of Thr187-phosphorylated p27 (Ref. 15). Concordantly, SKP2 depletion suppressed cone precursor proliferation and increased CC3 (Fig. 3a, Extended Data Fig. 5a). Notably, maturing cone precursors had exceptionally high Thr187-phosphorylated p27 (Extended Data Fig. 5c), coincident with a maturation-associated decrease in total p27 (Ref. 16), suggesting that SKP2-mediated p27 degradation might enable cone precursor proliferation. Consistent with this view, cone precursor proliferation was suppressed by ectopic p27 and enhanced by ectopic SKP2 or p27 knockdown (Fig. 3b, Extended Data Fig. 5b), as in retinoblastoma cells[15]. Thus, Rb-depleted cone precursors and retinoblastoma cells had similar signaling requirements.

We also assessed roles of the Rb-related p107 and p130. In mouse models, retinal tumorigenesis required loss of Rb combined with loss of p107, p130, or p27 (Refs. 10, 17). However, in human retinoblastomas, *p130*/*RBL2* losses are common, whereas *p107*/*RBL1* losses are rare[18] (Extended Data Fig. 6a). Moreover, whereas maturing cone precursors had abundant p130 and minimal p107, retinoblastomas had barely detectable p130 yet prominent p107 (Fig. 4b, Extended Data Fig. 6b), implicating p130 but not p107 in retinoblastoma suppression. Concordantly, co-knockdown of p130 with Rb increased cone precursor proliferation (Fig. 3a, Extended Data Fig. 5a, d) and p130 overexpression suppressed cone precursor and retinoblastoma cell proliferation (Fig. 3b, c, e). Meanwhile, p107 knockdown suppressed proliferation both in Rb-depleted cone precursors (Fig. 3a; Extended Data Fig. 5a, d) and in retinoblastoma cells (Fig. 3d–e; Extended Data Fig. 5e,g). In Y79, p107 knockdown decreased expression of MYCN and SKP2, while increasing the SKP2 target, p27 (Fig. 3e). These effects were seen with two shRNAs and were rescued by p107 restoration (Fig 3d,e, Extended Data Fig. 5d–i). Furthermore, p107 overexpression enhanced proliferation of retinoblastoma cells while suppressing that of neuroblastoma cells (Extended Data Fig. 5h–j). Thus, both in Rb-depleted cone precursors and in retinoblastoma cells, p130 suppressed proliferation whereas p107 had a proliferative role distinct from its function in mouse models.

After several months, some Rb- or Rb/p130-depleted cone precursor cultures formed suspension aggregates resembling retinoblastoma cells (Extended Data Fig. 7a). Rb/p130-depleted cultures proliferated more robustly and longer than those with Rb depletion alone, consistent with *p130* losses in many retinoblastoma cell lines (Extended Data Fig. 6a). The cultures had properties consistent with Rb/p130-depleted cone precursors (Extended Data Fig. 7b–h). When engrafted either 3 months or within one week after knockdown, Rb- or Rb/p130-depleted cone precursors formed retinoblastoma-like tumors in subretinal xenografts (Fig. 4a; Extended Data Fig. 8, 9). For cells engrafted within one week, tumors appeared within 6–14 months (Extended Data Fig. 8b), similar to the time needed to form tumors in children.

Cone precursor-derived tumors had differentiated histology, little Rb or p130, many $Ki67^+$ cells, and prominent p107 and SKP2, consistent with robust proliferation (Fig. 4a, b; Extended Data Fig. 9). They expressed the photoreceptor-related CRX, CD133, and IRBP and the cone-specific cone arrestin, L/M-opsin, and RXRγ; all at levels similar to retinoblastomas and developing retinas (Fig. 4b, Extended Data Fig. 9). This accords with the many cone-specific proteins in retinoblastoma tumors (Ref. 7, Supplementary Table 1). As in human retinoblastomas[7], cone precursor-derived tumor cells lacked numerous markers of other retinal cell types and had rare S-opsin and rhodopsin expression (Extended Data Fig. 10). Rb-depleted and Rb/p130-depleted cone precursor tumors also had structures resembling Flexner-Wintersteiner rosettes and fleurettes (Fig. 4a), which are retinoblastoma hallmarks[19]. Transmission electron microscopy confirmed the rosettes, with mitochondria positioned between the nuclei and rosette lumens (Fig 4c). Dense core vesicles were not seen in two Rb-depleted cone precursor tumors nor in two retinoblastomas, consistent with the reported rarity of such structures[20,21]. Finally, SNP-array analyses of two tumors revealed no megabase-size gains or losses, whereas qPCR analyses revealed a partial *RB1*

loss but not other frequently reported changes (Extended Data Fig. 8c–e), consistent with the lack of DNA copy number alterations in some retinoblastomas[22–24]. Thus, cone precursor tumors resembled human retinoblastomas at the histologic, ultrastructural, retinal marker, and molecular cytogenetic levels.

This study examined collaboration between Rb loss and retinal cell type-specific circuitries. We found that the circuitry of maturing L/M-cone precursors was uniquely conducive to proliferation and development of retinoblastoma-like tumors. While we cannot exclude the possibility that Rb loss could induce a cone program and proliferation in other cell types, the robust responses of the most highly enriched cone precursor populations and of cells in an intact fovea suggest that cone precursors are the primary if not the sole responding cell type. Cone precursor features that collaborated with Rb loss included cone lineage factors (TRβ2, RXRγ), highly expressed oncoproteins (MYCN and MDM2), and p27 down-regulation likely mediated by SKP2. Some of these features may be interdependent, as RXRγ promoted MDM2 expression[7], yet the larger program and its developmental purpose are unknown. Importantly, Rb-depleted cone precursor tumors had differentiated histology and lacked gross DNA aberrations, similar to putative early retinoblastoma elements[25]. These findings support a model in which Rb-deficient cone precursors form differentiated retinoblastomas, then dedifferentiate (Fig. 4d) and possibly acquire non-cone features[8,22]. Much of the circuitry implicated in cone precursor tumor initiation was also needed for retinoblastoma cell proliferation[7,15], suggesting that tumor cells can be addicted to the cancer-predisposing circuitry of their originating cell types.

METHODS

Retinoblastoma and retinal cell culture

Retinoblastoma cell lines Y79 and Weri-RB1 were obtained from the ATCC. RB177 was from an early passage culture and its identity confirmed by *RB1* mutation sequencing. Retinoblastoma cells were confirmed free of mycoplasma and cultured in RB culture medium (Iscove's Modified Dulbecco's Medium (IMDM), 10% fetal bovine serum (FBS), 55 μM beta-mercaptoethanol, with glutamine, penicillin, streptomycin, fungizone, and 10μg/ml Plasmocin (Invivogen)[7,26]). Fetal eyes were obtained with informed consent from the Human Fetal Tissue Repository of the Albert Einstein College of Medicine and from Advanced Bioscience Resources, Inc. under protocols approved by the Memorial Sloan-Kettering Cancer Center (MSKCC) Institutional Review Board, the Albert Einstein College of Medicine Institutional Review Board, and the Children's Hospital Los Angeles Committee on Clinical Investigations. After transport in IMDM with 10% FBS on ice, eyes were rinsed in 70% ethanol for 3 seconds and washed in sterile phosphate buffered saline (PBS). Eyes were opened using a sterile scalpel and lens removed. Retinas were detached using forceps and incubated in papain solution (Worthington Tissue Dissociation Kit) for 10–30 minutes at 37° C and 5% CO_2, with pipette mixing every 5 minutes. After dissociation to ~20-cell clusters, cells were diluted with 10 volumes of PBS and collected by centrifugation at 2,000 rpm (Sorvall, Legend RT), re-washed in PBS (all centrifugations at 2,000 rpm unless otherwise stated), suspended in RB culture medium as above, incubated at 37°C with 5% CO_2 overnight, and frozen in RB culture medium containing 10% DMSO.

Supernatant was transferred into a sterile container after each centrifugation and re-spun to prevent retinal cell losses. For lentivirus infections, cells were recovered from liquid nitrogen, cultured overnight, washed with PBS, suspended in 0.05% trypsin/EDTA (Cellgro) for 3–10 minutes with gentle pipetting, re-centrifuged, suspended in RB culture medium as above, and immediately infected. Cultures were maintained at high density, typically 50,000 cells/well (24-well dish) for unsorted cultures, with media changes every three days.

Fluorescence-activated cell sorting

Approximately 10 million dissociated retinal cells (~5 million per retina) were cultured for 18 h after thawing in RB culture medium, collected by centrifugation, washed with PBS, digested with 5 ml warm 0.05% trypsin/EDTA for 5–15 minutes while triturating in a 24-well culture plate 20 – 30 times per minute using a 1000 µl tip and checking every ~ 3 minutes, to produce 90–95% single cells, centrifuged as above (retaining the supernatant to prevent cell loss), suspended in 400 µl 5% FBS in PBS, and incubated at room temperature for 10 minutes. 100 µl of cells were combined with 100 µl 4 µg/ml of mouse IgG (Sigma, I-8765), 300 µl of cells were combined with 300 µl of pre-mixed anti-CD133-PE (Miltenyi Biotec, 130-080-801) at 1:6 and anti-CD44 FITC (Clone IM7, Abcam ab19622 or BD Biosciences, BDB553133) at 1:25, to give 1:12 CD133 and 1:50 CD44 final dilutions. After one hour at room temperature, cells were diluted with 900 µl 5% FBS in PBS, centrifuged as above, suspended in 500 µl 5% FBS/PBS with 300 ng/ml 4′, 6′-diamino-2-phenylindole (DAPI) and held on ice until sorting. Cells were sorted using a Becton-Dickenson FACSAria SORP with 100 mW 488 nm laser, the triple bandpass filter removed in the FITC channel, FACSDiva v8.0 software, and selecting live single cells based on forward scatter (FSC) width, side scatter (SSC) width, and DAPI exclusion. On FSC/SSC plots, cells were divided into small, medium, and large size groups and evaluated for CD133-PE and CD44-FITC. Eight populations collected into 500 µl complete medium as above were small, medium, and large $CD133^{hi}$, $CD44^{(-)}$; small, medium, and large $CD133^{lo}$, $CD44^{+}$; small $CD133^{(-)}$, $CD44^{(-)}$; and ungated live single cells. Each population was cultured in 50% Y79-conditioned medium with fungizone (50% fresh RB culture medium combined with 50% filtered Y79-conditioned RB culture medium), and half of the volume changed with fresh 50% Y79-conditioned medium every three days. Sorted populations were characterized by adhering cells to poly-L-lysine-coated coverslips (1,000–2,000 cells each) for 3 hours, fixing in 4% paraformaldehyde (PFA) for 5 minutes, washing in PBS four times, and storing at −20 degrees until immunostaining. Lentivirus infection was performed within 24 hours after sorting.

Lentiviral shRNA and cDNA expression constructs

pLKO lentiviral shRNA vectors from the TRC library (Open Biosystems/Thermo Scientific or MSKCC SKI High-Throughput Drug Screening and RNAi Core Facility)[27] were designated by “sh” followed by the name of the target gene and last 3–4 digits of the TRC or SKI identification numbers (Supplementary Table S2). *TRβ2* shRNA vectors were designed using Invitrogen BLOCK-iT™ RNAi Designer (http://rnaidesigner.invitrogen.com/rnaiexpress/) and siDirect (http://genomics.jp/sidirect/) and cloned using the TRC cloning strategy (www.addgene.org/pgvec1?f=v&cmd=showfile&file=protocols) with deoxyoligonucleotides for DNA-directed RNAi (Integrated DNA Technologies). They are

designated according to the position of the first shRNA target nucleotide after the translation initiation site (Supplementary Table S2). The pLKO scrambled control was Addgene plasmid 1864 (Ref. 28). pLKO-YFP-sh*RB1-733*, pLKO-YFP-sh*RB1-737*, and pLKO-YFP-SCR control virus were produced by replacement of puromycin resistant gene with YFP cDNA using In-Fusion cloning (Clontech), and generously provided by Zhengke Li. The lentiviral cDNA expression vector BE-Neo (BN) was created by replacing the *EGFP* gene of BE-*GFP*[29] with the *NeoR* gene between the EcoRI and BamHI sites (with assistance of Sarang Puranik). BN-*p130* was produced by inserting human *RBL2/p130* cDNA between the BE-Neo PshAI and XbaI site. BN-*SKP2* and BN-p107 were produced by inserting human *SKP2* or *RBL1/p107* cDNA respectively between the BsiWI and PspXI sites of BE-Neo. Since shRBL1-2621 (shp107-1) targets the 3′ untranslated region, only the *RBL1* ORF was cloned into BE-Neo to produce shRBL1-2621 resistant BN-p107. To produce shRBL1-2623 (shp107-2) resistant BN-p107-2r, the sh*RBL1* target sequence ‘gcagtgaataaggagtatgaa’ was mutated to ‘gcagtAaaCaaAgaAtatgaa’ without amino acid sequence changes using In-Fusion cloning (Clontech). BE-p27 was as described[15].

Lentivirus production and infections

Lentiviruses were produced by reverse transfection of suspended 2×10^7 293T cells using 20 μg lentiviral vector, 10 μg pVSV-G, 20 μg pCMV-dR8.91,(Ref. 30) and 100 μl Polyjet (SignaGen) or Lipofectamine 2000 (Life Technologies) in 15 cm dishes. The 3 ml plasmids–Polyjet complex and 1.5 ml 293T cell suspension were mixed in 50 ml centrifuge tubes and shaken for half hour before transferred to dishes. Virus harvested 48 and 72 h after transfection was combined, concentrated 50–100-fold by centrifugation at 25,000 rpm for 90 minutes, and suspended in RB culture medium. 500–2,000 μl of concentrated virus was used to infect 5×10^5 Y79, Weri-1, or RB177 retinoblastoma cells, or to infect 5×10^5 total retinal cells or 1×10^5 of each sorted retinal cell population in 500 μl of filtered conditioned RB culture medium in the presence of 4 μg/ml polybrene (Sigma-Aldrich) followed by gentle pipetting 25 times and shaking for 10 minutes in the hood. After 18 hours, cells were diluted in an equal volume of conditioned RB culture medium and maintained at 37° C with 5% CO_2. For co-infections, 100 μl of each concentrated virus was used to infect 1×10^4 total retinal cells or 1×10^3 sorted retinal cells suspended in 100 μl of conditioned RB culture medium with 4 μg/ml polybrene in a total volume of 300 μl, and medium was replaced with 150 μl 50% Y79 and other RB cell conditioned medium 24 h post-infection. Infected cells were selected starting 48 h after infection with 1.4 – 3 μg/ml puromycin for 48–72 h or with 50–100 μg/ml G418 for 4–7 days, and fed every 2–3 days by replacing two-thirds of the media with 50% Y79 and other RB cell conditioned medium.

Intact FW19 retinas were infected either 1) within the globe, by cutting a cross section through the cornea, removing the lens and most of the vitreous, and pipetting 500 μl of concentrated pLKO versions of sh*RB1-733* and sh*RB1-737* or scrambled control lentivirus into the sub-retinal space and vitreous (causing retinal detachment) in a 24-well plate with the globe submerged in RB culture medium with 1 ml lentivirus suspension, followed after two days by addition of 2 ml of freshly prepared concentrated lentivirus; or 2) after removal of the intact retina and residual vitreous in a 12 well plate, by addition of 1 ml of 80X concentrated pLKO-YFP-sh*RB1-733* or scrambled control lentivirus, reinfection with the

same viruses one and three days later, and changing 50% of medium with a 1:1 mixture of fresh and ocular globe-conditioned medium daily thereafter. Displaced retinal tissue was fixed with 2% PFA/PBS for 2 hours at 4° C, and eyes with remaining tissue were fixed in 2% PFA/PBS overnight at 4° C. Tissue samples were washed with PBS, transferred to 30% sucrose in PBS, and embedded in 30% sucrose/PBS:OCT at a 2:1 ratio, and cryosectioned at 8–10 μm.

Real time quantitative PCR

Total RNA was isolated using StrataPrep® total RNA microprep kit (Stratagene) for < 1,000 cells (in FACS isolated populations) or GenElute™ Mammalian Total RNA Miniprep Kit (Sigma) for all other analyses. cDNA was synthesized using ImProm-II™ Reverse Transcription System (Promega). Primers were designed by Beacon Designer software (Premier Biosoft International) or Primer3 (http://frodo.wi.mit.edu/primer3/) (Supplementary Table S3). Relative mRNA levels were determined by qPCR using QuantiTect SYBR Green PCR Kit (Qiagen) or Maxima® SYBR Green qPCR Master Mix (Fermentas) on an Applied Biosystems ABI 7900HT Sequence Detection System or ViiA™ 7 Real-Time PCR System using 95°C 10 min followed by 40 cycles of 95°C 20 seconds, 54°C 30 seconds, 72°C 30 seconds. Each sample was evaluated in triplicate and normalized to *ACTB* and *GAPDH*. Values represent the averages of both normalized results and error bars the standard deviation.

Immunostaining

Antibodies—Antibodies are described in Supplementary Table S4.

Sample Preparation—Eyes were prepared and cryosectioned as described[7,16]. Cultured retinal cells were dissociated by gentle triturating, spread on poly-L-lysine coated slides, incubated in a humidified incubator at 5% CO_2 and 37 °C for 3h, fixed in 4% PFA/PBS for 5 min, gently rinsed with PBS 4 times, vacuum-dried for 5 min, and stored at −20 °C.

Co-staining strategies—The following co-staining combinations and orders were used to assess Ki67 expression in different retinal cell types. For cones: 1a. Mouse anti-cone arrestin,[31] anti-mouse-biotin, streptavidin-FITC, rabbit anti-Ki67, anti-rabbit-Cy3, rabbit anti-CRX, anti-rabbit-Cy5. 1b. Mouse anti-Ki67, anti-mouse-Cy3, rabbit anti-CRX, anti-rabbit-FITC, rabbit anti-human cone arrestin[32], anti-rabbit-Cy5. 2. Mouse anti-Ki67, anti-mouse-biotin, streptavidin-FITC, rabbit anti-CRX, anti-rabbit Cy3, rabbit anti-L/M-opsin, anti-rabbit-Cy5. 3. Mouse anti-RXRγ, anti-mouse-biotin, streptavidin-FITC, rabbit anti-Ki67, anti-rabbit-Cy3, rabbit anti-CRX, anti-rabbit-Cy5. For progenitors, Müller, and horizontal amacrine cells: Mouse anti-Pax6, anti-mouse-biotin, streptavidin-FITC, rabbit anti-Ki67, anti-rabbit-Cy3, rabbit anti-nestin, anti-rabbit-Cy5. For other retinal cell types: mouse anti-human Ki67, anti-mouse-biotin, streptavidin-FITC, and rabbit antibodies for retinal specific markers, anti-rabbit Cy3. For BrdU labeling, 10 μM BrdU was added to medium for 2 hours on day 23 after Rb knockdown and cells stained with rat anti-BrdU, anti-rat-FITC, rabbit anti-CRX, anti-rabbit-Cy3, rabbit anti-L/M-opsin, anti-rabbit-Cy5.

Co-staining with mouse antibodies—Sections or cells were treated with 1 mM EDTA/PBS for 5 min at room temperature and washed with PBS. Sections were treated with ABC kit reagent A (Vector Laboratories, Burlingame, CA) in PBS for 15 min, washed in PBS, treated with ABC kit reagent B (Vector Laboratories) in PBS for 15 min, washed in PBS, blocked and permeabilized for 20 min in super block (2.5% horse serum, 2.5% donkey serum, 2.5% human serum, 1% BSA, 0.1% Triton-X-100, and 0.05% Tween-20 in PBS; filtered with 0.22 μm filter), incubated in mouse primary antibody in super block overnight at 4°C, washed in PBS, incubated in biotinylated horse anti-mouse antibody in super block for 30 min, washed in PBS, incubated with FITC-conjugated streptavidin in PBS, and washed with PBS.

Co-staining analyses with other antibodies—On completing the first staining reaction as above, sections were incubated in super block for 20 min, incubated overnight with primary antibody in super block, washed in PBS, incubated with Cy3- or Cy5-conjugated secondary antibody in super block for 30 min, and washed in PBS. Sections were then stained with 1 μg/ml DAPI in PBS, dried, mounted in Vectashield (Vector Labs), and imaged using an Axioplan2 (Carl Zeiss MicroImaging, LLC) or confocal DMIRE2 (Leica, Wetzlar, Germany) microscopes. Antibody specificity was confirmed by staining in parallel with control IgG or no primary antibody.

Interpretation of immunostaining—Antibody-dependent immunofluorescence signals were distinguished from autofluorescence by virtue of signal detected in only one color channel. Cells with autofluorescence in multiple channels or with DNA condensation, fragmentation, or degradation were excluded. Cytoplasmic autofluorescence common in astrocytes, Muller glia, and ganglion cells was distinguished from authentic antigens by its detection at multiple wavelengths in cells with characteristic glial cytoplasmic and nuclear morphology. Non-specific cytoplasmic staining by concentrated nestin antibody was distinguished from authentic nestin staining by its homogeneous rather than fiber-like structure. Non-specific nuclear staining of L/M-opsin was avoided by using reduced antibody concentration.

EdU labeling and detection

Click-iT EdU Alexa Fluor 488 Imaging Kit was used for EdU labeling to detect proliferation. Dissociated or sorted retinal cells were infected with shRB1 or control lentivirus. After 14 days, 20 μg/ml of EdU was added into medium and incubated for 1 hour; the cells were attached on poly-L-lysine-coated coverslips for 2 hours and fixed for 5 minutes. The cells were blocked and permeabilized for 20 min in super block as above and EdU was detected by addition of Click-iT® reaction cocktails containing 2 μM Alexa Fluor 488 azide for 1 hour. Co-staining was performed after EdU labeling with different combination of antibodies for retinal cell markers and secondary antibodies conjugated with Cy3 or Cy5, described as above. For cones, cone arrestin-Cy3 + CRX-Cy5, RXRγ-Cy3 + CRX-Cy5, and L/M-opsin-Cy3 + CRX-Cy5 were utilized for co-staining with EdU.

Immunoblotting

Cells were washed in PBS, lysed in ELB+ (150 mM NaCl, 50 mM HEPES pH 7.4, 0.1% NP40, 5 mM EDTA, 2 mM DTT, 1 mM phenylmethylsulfonyl fluoride, 10 mM NaF, 1 mM NaVO4, Thermo Scientific Halt phosphatase inhibitor cocktail and protease inhibitor cocktails), separated on 4–20% Ready Gel polyacrylamide gels (Jule Biotechnologies INC) or 8% polyacrylamide (for Rb western), and transferred to Hybond-ECL nitrocellulose membrane (Amersham). Membranes were probed with antibodies (Supplementary Table S4) and developed using horseradish peroxidase-conjugated anti-mouse or anti-rabbit antibodies and the ECL Advance Western Blotting Detection Kit (Amersham Biosciences) or Thermo Scientific SuperSignal-West Femto Chemiluminescent Substrate, and HyBlot CL X-Ray film (Denville Scientific).

Xenografts

All animal experiments complied with ethical regulations and were approved by the MSKCC Institutional Animal Care and Use Committee. Xenografts were performed on 6-week-old male athymic (*Foxn1*$^{-/-}$) mice (Taconic, Hudson, NY) or 6-week-old male *Nod/Scid/Il2rγ−/−* mice (Jackson Laboratories). Cultured cells were dissociated by pipetting, suspended in RB growth medium at 5×10^4 cells/μl (day 90) or 2.5×10^3 cells/μl (days 3 or 7), held on ice, and 2 μl injected into the subretinal space as described[7]. Irradiated 5053 rodent diet with amoxicillin was provided from 2 days before to two weeks after injection to prevent infection. Some tumor-bearing eyes were fixed and embedded as described[7,16].

DNA copy number analyses

Genomic DNA from retinoblastomas, cone-derived retinoblastoma-like cells, and cone-derived xenograft tumors were isolated with QiaAMP DNA Mini kit (Qiagen). Genomic DNA of cone-derived cells was digested with XhoI to separate pLKO DNA hairpin structures. Relative DNA levels were determined in triplicate by qPCR using QuantiTect SYBR Green PCR Kit (Qiagen) on an Applied Biosystems ABI 7900HT Sequence Detection System or ViiA™ 7 Real-Time PCR System, using primers listed in Supplementary Table S5 and normalizing to the average of the *HNF4a* and *BRCA1* genes. Integrated pLKO-sh*RB1-733*, sh*RB-737*, and sh*RBL2-923* copy numbers were analyzed using primers corresponding to the pLKO.1 U6 promoter and *RB1*- or *RBL2*-specific shRNA sequences. High resolution SNP-array DNA copy number analyses were performed using CytoScan® HD (Affymetrix, 901835). Data were analyzed using Chromosome Analysis Suite 2.0 (Affymetrix).

Statistical Analyses

Measurements were performed in triplicate and differences between means assessed for significance using Student's t-test. Sample sizes were chosen based upon the maximum cell numbers that could be utilized for individual experiments given sample availability.

Transmission electron microscopy

Human retinoblastomas and cone-derived xenograft tumors were fixed with 4% PFA in PBS, rinsed in 0.1 M sodium cacodylate buffer, post-fixed in 2% Osmium Tetroxide for one

hour, rinsed in distilled water, dehydrated in a graded series of 50%, 75%, 95%, and 100% ethanol, followed by two 10-minute incubations in propylene oxide and overnight incubation in 1:1 Propylene oxide/Poly Bed 812. The samples were embedded in Poly Bed 812 and cured at 60° C. Ultra-thin sections were obtained with a Reichert Ultracut S microtome. Sections were stained with Uranyl Acetate and Lead Citrate and photographed using a Jeol 1200EX Transmission Electron microscope.

Extended Data

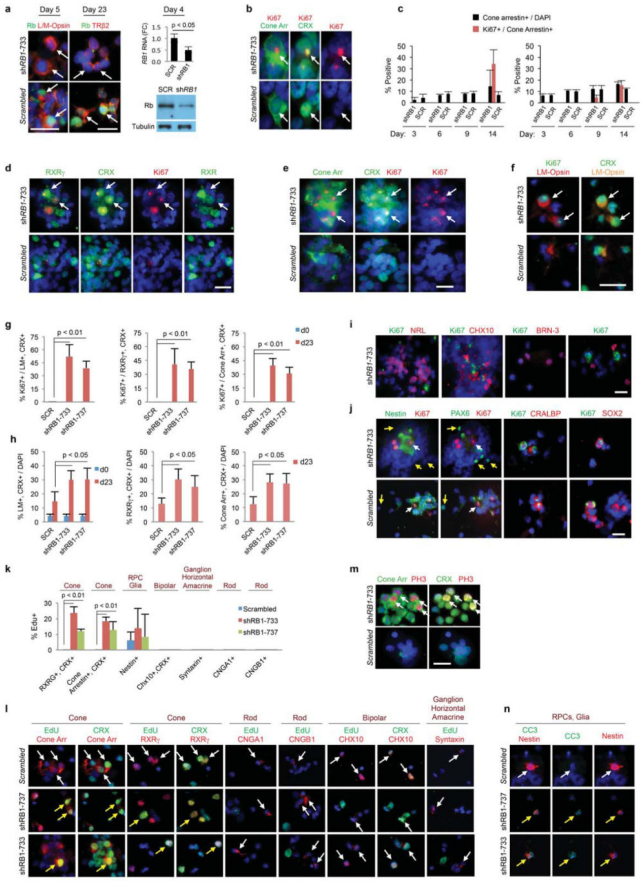

Extended Data Figure 1. Proliferation of cone-like cells after Rb depletion in dissociated FW19 retina

a, Decreased Rb protein in L/M-opsin$^+$ or TRβ2$^+$ cells (arrows) on days 5 or 23, and decreased *RB1* RNA or Rb protein on day 4 after sh*RB1-733* transduction. **b**, Cone arrestin$^+$, CRX$^+$ cells (arrows) with or without Ki67 co-expression. **c**, Ki67$^+$, cone arrestin$^+$ cells first detected 9 or 14 days post-transduction in two experiments. **d**–f Co-staining of Ki67 with RXRγ/CRX at 14 days, (**d**) with cone arrestin/CRX at 14 days (**e**), or with L/M-opsin/CRX at 23 days (**f**) after transduction with sh*RB1-733* or a scrambled control. **g**, Percentage of cells co-expressing Ki67 with L/M-opsin/CRX, RXRγ/CRX, or cone arrestin/CRX, 23 days post-transduction. **h**, Prevalence of cells co-staining for L/M-opsin/CRX, RXRγ/CRX, or cone arrestin/CRX 23 days post-transduction. **i**, Ki67 not detected in cells expressing markers of rods (NRL), ganglion cells (BRN-3), bipolar cells (strong CHX10), or horizontal

cells (PROX1) 14 days post-transduction. **j**, Co-expression of Ki67 with markers of RPCs (nestin, white arrows) or Müller glia (CRALBP or SOX2), but not in $PAX6^{+}$, $nestin^{(-)}$ ganglion, amacrine, or horizontal cells (yellow arrows) 14 days post-transduction. **k–l**, EdU incorporation in cells expressing markers of cones (cone arrestin/CRX or RXRγ/CRX, yellow arrows in **l**) but not in cells expressing markers of rods (CNGA1, CNGB1), bipolar cells (CHX10/CRX), or ganglion, horizontal, or amacrine cells (syntaxin) (white arrows in **l**) 14 days after transduction. Black lines above labels demarcate distinct fields. **m**, Co-staining of phosphohistone H3 (PH3) with cone arrestin/CRX 23 days post-transduction. **n**, Apoptosis marker CC3 in cells expressing RPC and glial marker nestin 14 days after transduction with *RB1*-directed shRNAs (yellow arrow) but not with scrambled control (white arrow). Values and error bars are means and standard deviation of triplicate assays for all Extended Data figures. Scale bars, 20 μm. Data are representative of at least two independent experiments.

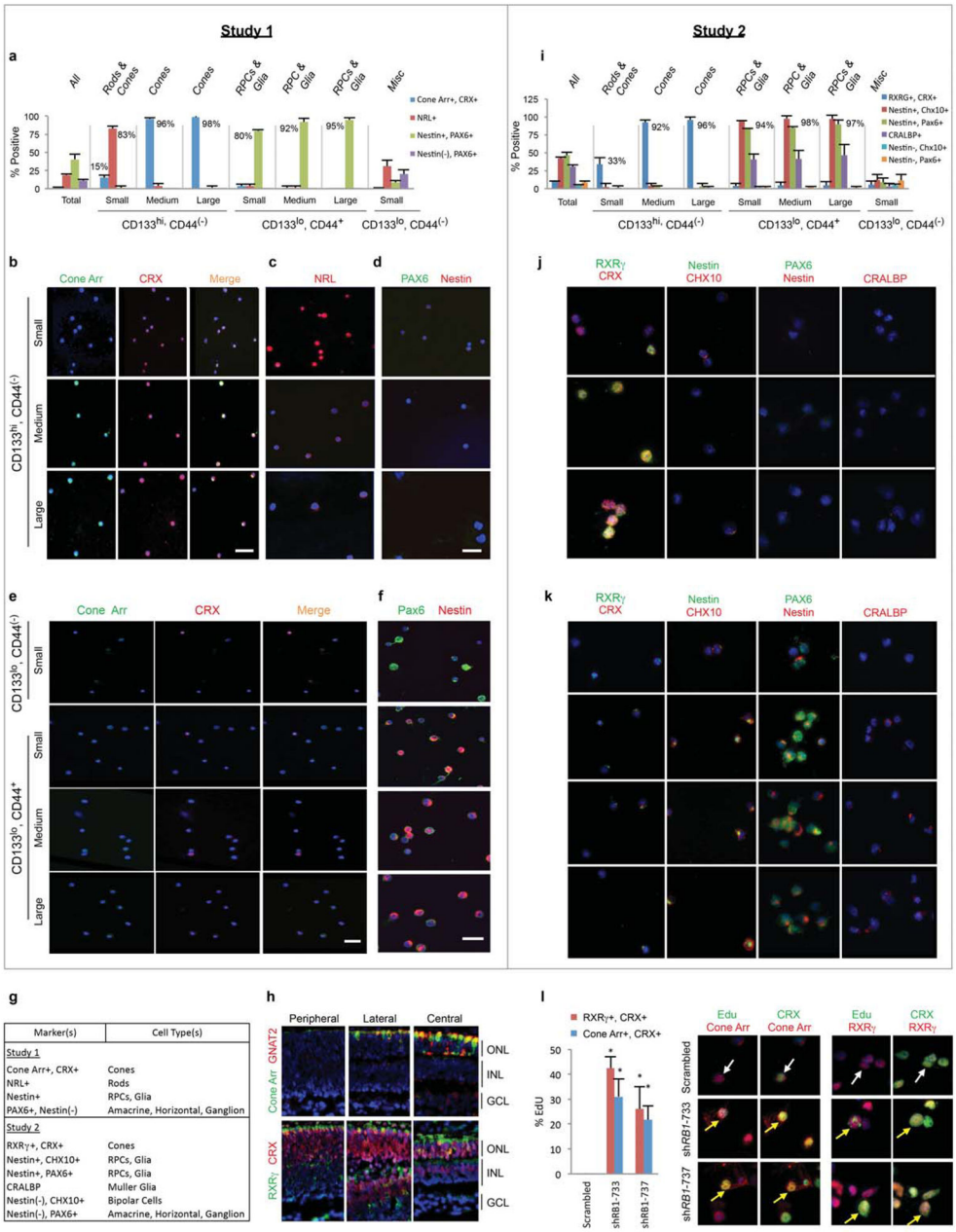

Marker(s)	Cell Type(s)
Study 1	
Cone Arr+, CRX+	Cones
NRL+	Rods
Nestin+	RPCs, Glia
PAX6+, Nestin(-)	Amacrine, Horizontal, Ganglion
Study 2	
RXRγ+, CRX+	Cones
Nestin+, CHX10+	RPCs, Glia
Nestin+, PAX6+	RPCs, Glia
CRALBP	Muller Glia
Nestin(-), CHX10+	Bipolar Cells
Nestin(-), PAX6+	Amacrine, Horizontal, Ganglion

Extended Data Figure 2. FACS isolation of retinal cell populations

Retinal cells were isolated according to size, CD133, and CD44 staining. In Study 1, cell type compositions in each fraction (**a)** were determined by immunostaining with cone arrestin/CRX (**b**, **e**), NRL (**c**), and nestin/PAX6 (**d**, **f**). In study 2, cell type compositions (**i**) were determined by immunostaining with RXRγ/CRX, nestin/CHX10, nestin/PAX6, and CRALBP (**j, k**). The percentages of the predominant cell types in each population (**a**, **i**) and marker specificities (**g**) are indicated. **h,** Cone-specific co-staining of cone arrestin and GNAT2 (*top*) and cone-specific co-staining of RXRγ and CRX (*bottom*) in FW19 retina. **l**, Co-staining of cells for EdU and cone arrestin/CRX or RXRγ/CRX 14 days after transduction of the cone-enriched medium plus large CD133^{hi}, CD44$^{(-)}$ population isolated

as in (i–k) with two *RB1* shRNAs (yellow arrows) but not with the scrambled control (white arrows). In both studies, CD133^{hi}, CD44$^{(-)}$ medium and large size populations mainly consisted of cells expressing cone markers (CRX/cone arrestin or CRX/RXRγ). The CD133^{hi}, CD44$^{(-)}$small population mainly consisted of cells expressing a rod marker (NRL) with a variable proportion expressing cone markers. All CD133^{lo}, CD44^{+} populations mainly consisted of cells co-expressing RPC and glial markers (nestin/PAX6, nestin/CHX10, or CRALBP). The CD133^{lo}, CD44$^{(-)}$ small size population consisted of cells with diverse immunophenotypes. Scale bars, 30 μm.

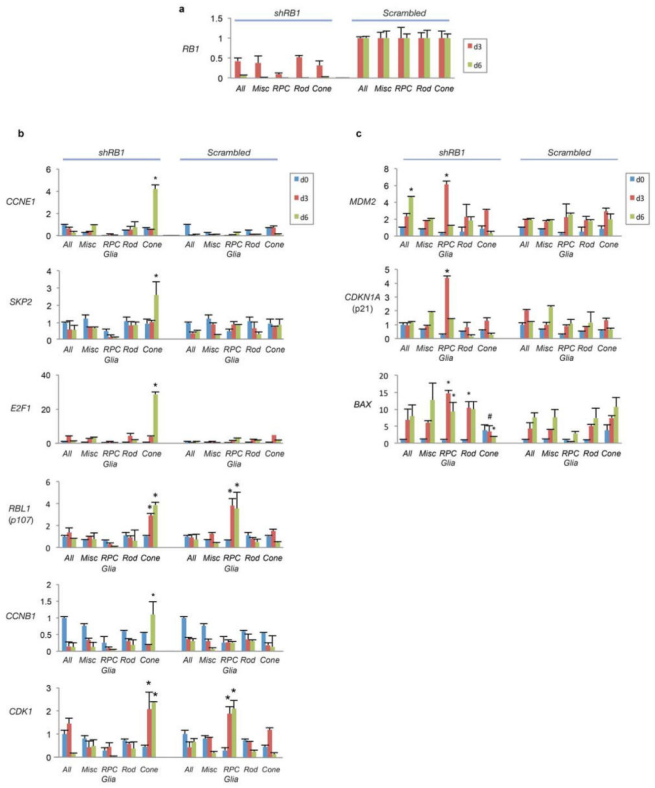

Extended Data Figure 3. Cone precursor gene expression response to Rb depletion

a–b, Fold change in RNA level relative to day 0 uninfected cells for (**a**) *RB1*, or (**b**) the indicated E2F-responsive genes, or (**c**) the indicated p53-regulated genes, 3 and 6 days after transduction of each population with a mixture of sh*RB1-733* and sh*RB1-737*, or with scrambled control. Comparing sh*RB1* and scrambled control: *, $p < 0.01$; #, $p < 0.05$. Data are representative of two sets of qPCR analyses.

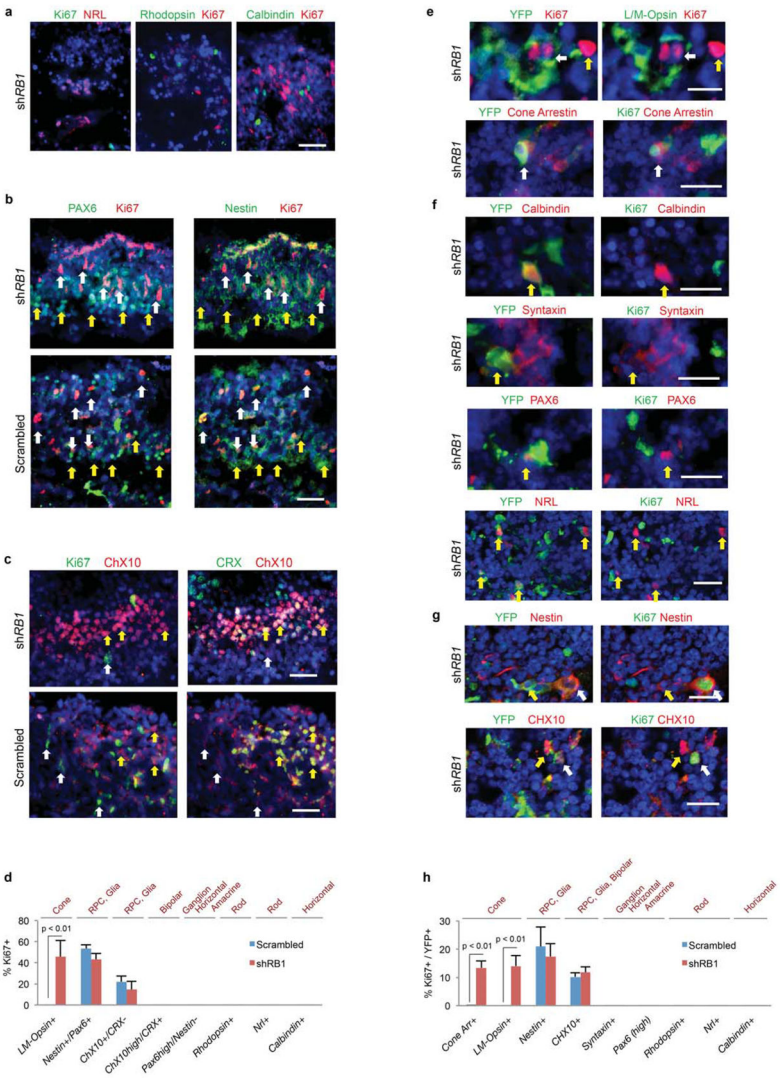

Extended Data Figure 4. Proliferation status of retinal cells other than cones 15 days after sh*RB1* transduction of intact FW19 retinas

a–c, Combined transduction with pLKO-sh*RB1-733* and *-737*. **a**, Ki67 not detected in NRL^{+}, or rhodopsin^{+} rod photoreceptors or in calbindin^{+} horizontal cells. **b**, Ki67 detected in PAX6^{lo}, nestin^{+} RPCs (white arrows) but not in PAX6^{hi}, nestin$^{(-)}$ horizontal, amacrine, or ganglion cells (yellow arrows). **c**, Ki67 detected in CHX10^{+}, CRX$^{(-)}$ RPCs (white arrows) but not in CHX10^{+}, CRX^{+} bipolar cells (yellow arrows). **d**, Percentage of cells co-expressing Ki67 and retinal cell markers. **e–h,** Transduction with yellow fluorescent protein-marked pLKO-YFP-sh*RB1-733*. **e**, Ki67 detected in YFP^{+}, L/M-opsin^{+} or YFP^{+}, cone arrestin^{+} cone precursors (white arrows) and in undefined YFP$^{(-)}$ cell (yellow arrow). **f**, Ki67 not detected in YFP^{+}, calbindin^{+} horizontal cells, YFP^{+}, syntaxin^{+} or YFP^{+}, PAX6^{+} amacrine cells, or in YFP^{+}, NRL^{+} rod precursors. **g**, Ki67 detected (white arrows) or not detected (yellow arrows) in YFP^{+}, nestin^{+} RPCs or glia, or in YFP^{+}, CHX10^{+} RPCs or bipolar cells. **h**, Proportion of Ki67^{+} cells co-expressing YFP and retinal markers after transduction with pLKO-YFP-sh*RB1-733* or scrambled control. Scale bars, 20 μm. Analyses

in a–d and in e–h represent two independent experiments. All Immunostaining was performed at least twice.

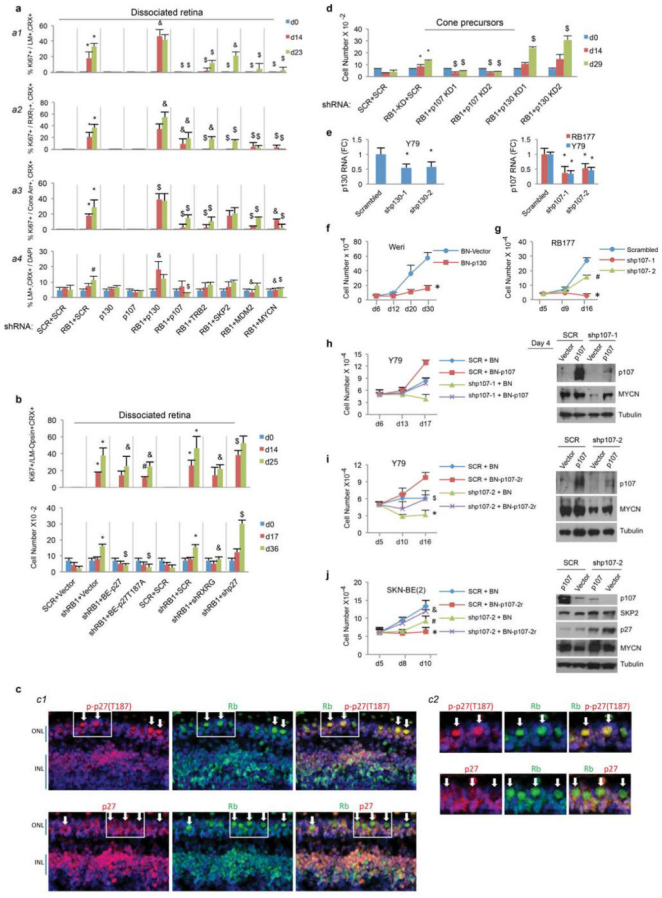

Extended Data Figure 5. Effect of cone- and Rb-related circuitry on cone precursor response to Rb depletion

a, Percentage of Ki67$^+$ cells among L/M-opsin$^+$, CRX$^+$ cells (*a1*), among RXRγ$^+$, CRX$^+$ cells (*a2*), or among cone arrestin$^+$, CRX$^+$ cells (*a3*); and percentage of L/M-opsin$^+$, CRX$^+$ cells among all cells with DAPI$^+$ nuclei (*a4*) after transduction of dissociated FW18 retina with sh*RB1-733* and shRNAs against p130, p107, TRβ2, SKP2, MDM2, and MYCN. **b**, Percentage of Ki67$^+$ cells among L/M-opsin$^+$, CRX$^+$ cone-like cells (*top*) and proliferative response (*bottom*) after transduction of dissociated FW18 retina with sh*RB1-733* and with shRNAs against RXRγ and p27 (shRNAs 856+930), or with overexpression of p27 and p27-T187A. **c**, High-level Thr187 phosphorylated p27 (p27-T187-Ph, *top*) coinciding with down-regulation of total p27 (*bottom*) and prominent Rb during cone precursor maturation. ***c1***, Perifoveal region of FW18 retina. ***c2***, Enlarged view of boxed regions in ***c1***. Arrows, cone precursors identified by large, strongly Rb$^+$ nuclei and lack of p27 signal in characteristic outer nuclear layer (ONL) position[7,16]. **d**, Effect of two *RBL1-p107* or two *RBL2-p130* shRNAs on proliferation of Rb-depleted isolated cone precursors. **e**, Knockdown efficacy of two *RBL1-p107* or two *RBL2-p130* shRNAs in Y79 and RB177 retinoblastoma cells. **f**, Impaired proliferation of Weri-RB1 retinoblastoma cells after

transduction with BN-p130 compared to vector control. **g**, Impaired proliferation of RB177 retinoblastoma cells following transduction with two *p107* shRNAs. **h**, **i**, Impaired proliferation and MYCN expression in Y79 cells following *p107* knockdown with two *p107*-directed shRNAs, and rescue by shRNA-resistant BN-*p107* constructs. **j**, p27 accumulation and growth suppression following *p107* knockdown with sh*p107-2* rescued by BN-*p107-2r* in *RB1*-wild type SKN-BE(2) neuroblastoma cells. p107 overexpression impaired SKN-BE(2) growth, contrary to its effects in Y79. Compared to SCR or Vector control: *, $P < 0.01$. #, $P < 0.05$. Compared to *RB1*-KD+SCR or RB1-KD+BN-Vector: $, $P < 0.01$; &, $P < 0.05$. Compared to shp107-2+BN-Vector: $, $P < 0.01$; &, P<0.05 (**h** and **i**). Data are representative of more than two independent experiments except for SKN-BE(2) analyses.

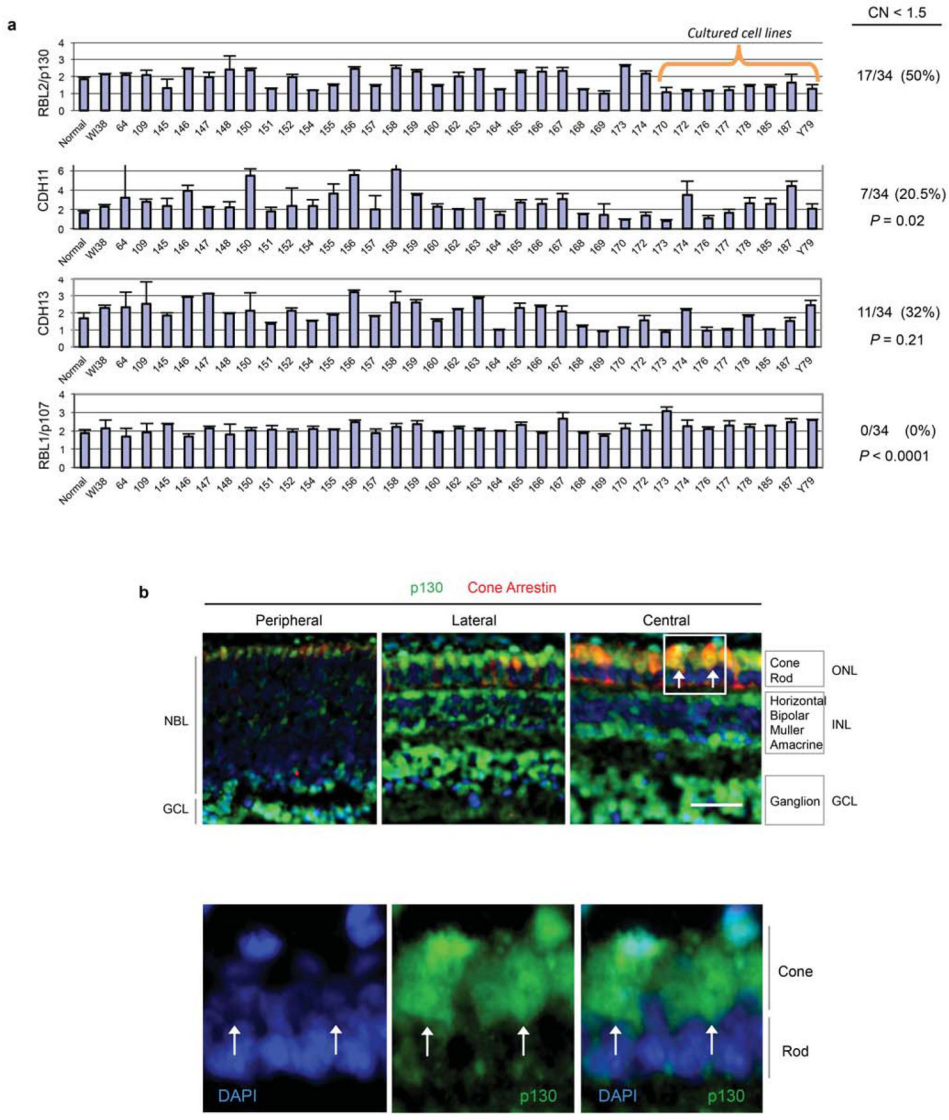

Extended Data Figure 6. p130 copy number in retinoblastomas and cone precursor expression

a, DNA copy number of *RBL2/p130*, other 16q genes implicated in retinoblastoma (*CDH11*, *CDH13*), and *RBL1/p107* determined by qPCR (n=6). The percentage of retinoblastomas with copy number (CN) < 1.5 was higher for *RBL2/p130* than for other 16q genes (summarized at *right*, P values relative to *RBL2/p130* using Fisher's exact test). **b**, p130 in peripheral, lateral, and central FW19 retina. Boxed region in maturing central retina (*top*) and enlarged view (*bottom*) show prominent p130 in weakly DAPI-stained cone precursor nuclei (arrows). Scale bars, 40 μm. Data are representative of at least two independent experiments.

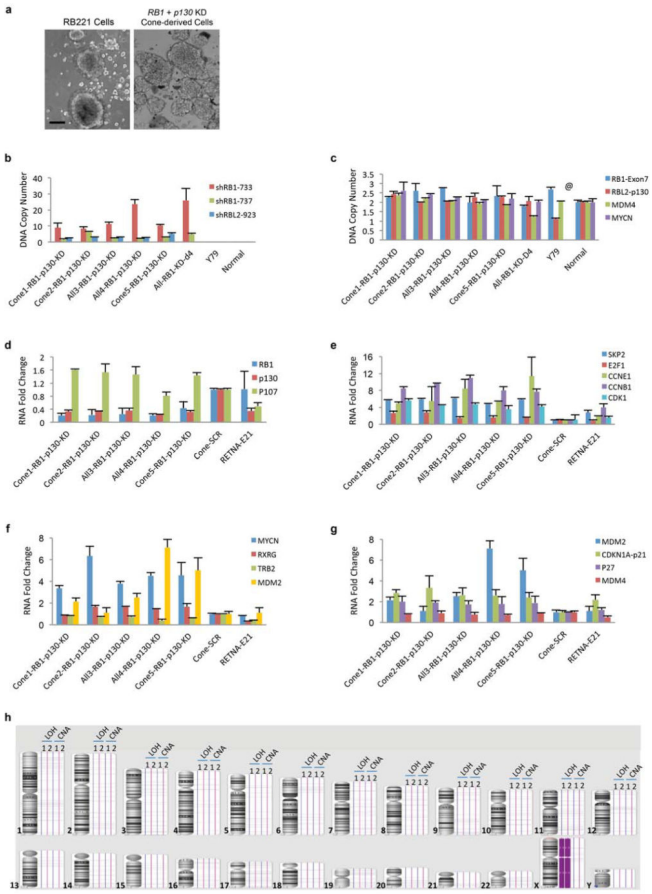

Extended Data Figure 7. Characterization of Rb/p130-depleted retinoblastoma-like cells

a, Similar appearance of Rb/p130-depleted cones and early passage retinoblastoma cells. Scale bars, 40 μm. **b–c,** DNA copy number of shRNA vectors (**b**) or selected genes (**c**) in cell lines derived from Rb/p130-depleted cone precursors (Cone1, Cone2, Cone5) or from Rb/p130-depleted unsorted retinal cells (All3, All4), in Rb-depleted unsorted retinal cells four days post-transduction (All-*RB1*-KD-d4), in Y79 cells, or in FW21 retina (Normal) (n=6). All cell lines retained *RB1* and *RBL2/p130* shRNA vectors and lacked *RB1* or *RBL2/p130* copy number alterations. @, Y79 *MYCN* copy number (~78) not shown. **d–g**, RT-qPCR gene expression analyses in the indicated cell lines relative to cones transduced with scrambled control or FW21 retina (n=6). **d**, All cell lines had diminished *RB1* and *RBL2/p130* expression. **e–g**, Altered expression of cell cycle related (**e**), cone-related (**f**), and

apoptosis related (**g**) genes. **h**, SNP-array analysis of two Rb/p130-depleted cone precursor cell lines (1, 2), revealing no megabase-size loss of heterozygosity (LOH) or copy number alterations (CNAs). Data are representative of at least two analyses (b–g) or analyses of two cell lines (h).

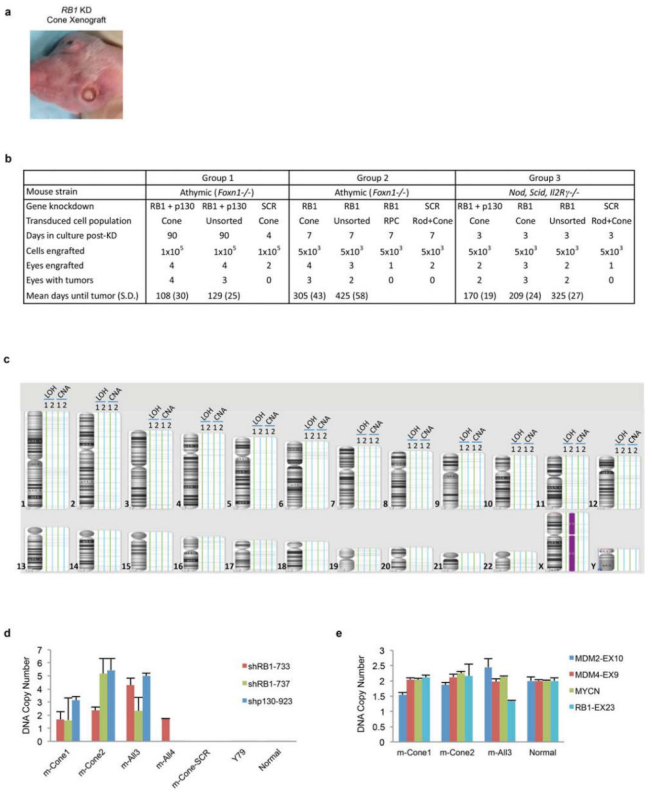

	Group 1			Group 2				Group 3			
Mouse strain	Athymic (*Foxn1-/-*)			Athymic (*Foxn1-/-*)				*Nod, Scid, Il2Rγ-/-*			
Gene knockdown	RB1 + p130	RB1 + p130	SCR	RB1	RB1	RB1	SCR	RB1 + p130	RB1	RB1	SCR
Transduced cell population	Cone	Unsorted	Cone	Cone	Unsorted	RPC	Rod+Cone	Cone	Cone	Unsorted	Rod+Cone
Days in culture post-KD	90	90	4	7	7	7	7	3	3	3	3
Cells engrafted	$1x10^5$	$1x10^5$	$1x10^5$	$5x10^3$	$5x10^3$	$5x10^3$	$5x10^3$	$5x10^3$	$5x10^3$	$5x10^3$	$5x10^3$
Eyes engrafted	4	4	2	4	3	1	2	2	3	2	1
Eyes with tumors	4	3	0	3	2	0	0	2	3	2	0
Mean days until tumor (S.D.)	108 (30)	129 (25)		305 (43)	425 (58)			170 (19)	209 (24)	325 (27)	

Extended Data Figure 8. Characterization of Rb- and Rb/p130-depleted cone precursor tumors

a, Intraocular tumor four months after Rb-depleted cone precursor xenograft. **b**, Summary of subretinal xenograft Groups 1, 2, 3. Sample size was as needed to assess tumor phenotypes. Mice were randomly assigned to different xenograft regimens and the investigator blinded to the assignment until the tumor analyses. Two mice with early death were excluded from the analyses. **c**, SNP-array analysis of one Rb/p130-depleted (tumor 1) or one Rb-depleted (tumor 2) cone precursor-derived tumors from xenograft Group 3, revealing no megabase-size LOH or CNAs. **d**, qPCR analysis of pLKO shRNA vector copy number in tumors derived from Rb/p130-depleted cone precursors (m-Cone1, m-Cone2) or from Rb/p130-depleted unsorted retinal cells (m-All3, m-All4), or in mouse ocular tissue (m-Cone-SCR), Y79 cells, or FW19 retina (Normal). All tumors retained sh*RB1* and/or sh*p130* vector sequences, confirming their engineered cone precursor origin. **e**, qPCR analysis of *MDM2*, *MDM4*, *RB1*, and *MYCN* copy number in three cone-derived tumors and normal retina (n=6). DNA copy number data (**d**, **e**) are representative of two analyses.

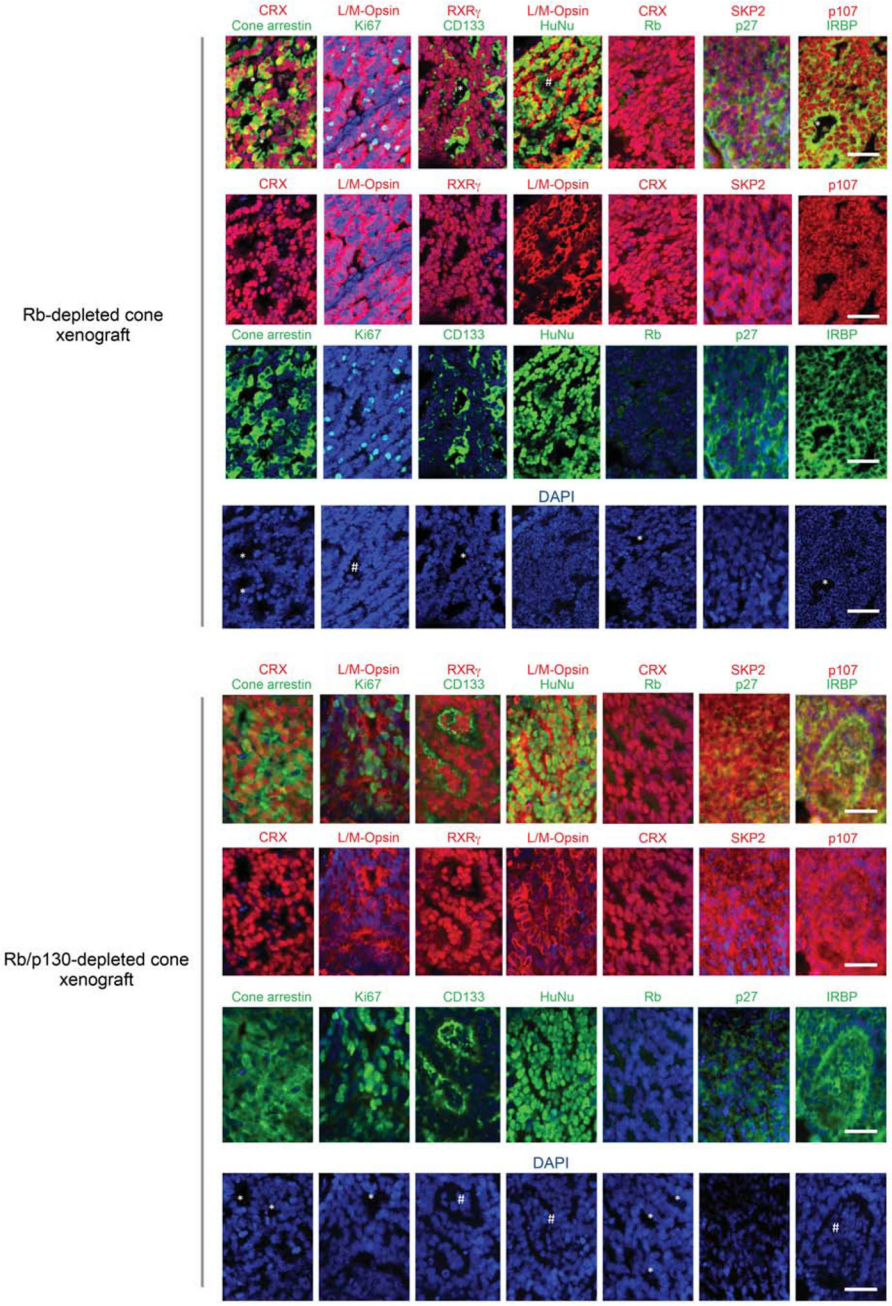

Extended Data Figure 9. Cone and cell cycle related proteins in Rb- or Rb/p130-depleted cone precursor tumors engrafted three days post-transduction

The vast majority of tumor cells expressed human nuclear antigen (HuNU), confirming their xenograft origin. They also expressed cone-related proteins (CRX, cone arrestin, L/M-opsin, RXRγ, CD133, and IRBP) and proliferation-related proteins (Ki67, SKP2, p107, and cytoplasmic p27) but lacked Rb. Tumors had elements resembling Flexner-Wintersteiner rosettes (*) and fleurettes (#). Scale bars, 40 μm. Data are representative of three independent experiments.

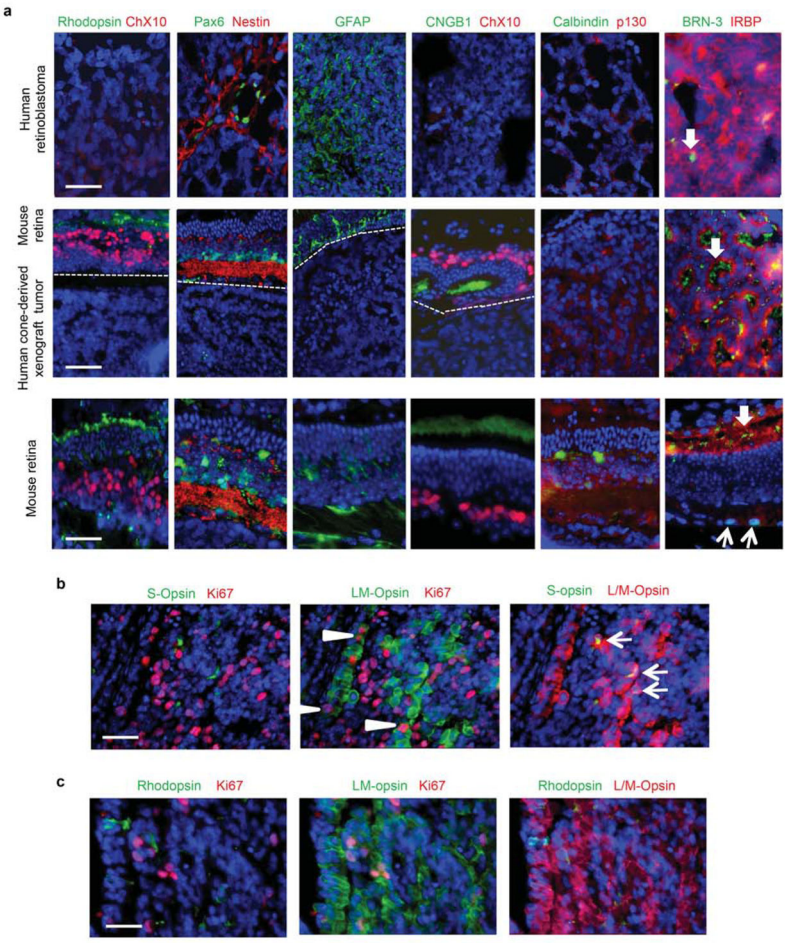

Extended Data Figure 10. Analysis of non-cone cell markers in cone precursor-derived tumors and retinoblastomas

a, Proteins detected in normal retina but not in cone-derived tumor or human retinoblastoma cells included markers of rods (rhodopsin, CNGB1), RPCs and Müller glia (nestin, GFAP, PAX6), bipolar cells (CHX10), ganglion, amacrine, and horizontal cells (calbindin, PAX6), and ganglion cells (nuclear BRN-3, thin arrows in mouse retina). $PAX6^+$, $nestin^+$ cells detected in human retinoblastoma were previously found to be Rb^+ non-tumor cells from tumor-associated retina[7]. An uncharacterized cytoplasmic BRN-3 signal (bold arrows) was detected in mouse photoreceptor outer segments and in cone-derived tumor and retinoblastoma rosettes. **b**, L/M-opsin was detected in most cone-derived tumor cells. However, rare cells co-expressed S-opsin and L/M-opsin (arrows), as in immature L/M-cone precursors and human retinoblastomas[7]. **c**, One tumor had rare $rhodopsin^+$, $Ki67^{(-)}$ cells but no detected $rhodopsin^+$, $Ki67^+$ cells, as in a previously characterized retinoma-like regions[7]. Scale bars, 40 μm. Data are representative of three independent xenograft experiments.

Supplementary Material

Refer to Web version on PubMed Central for supplementary material.

Acknowledgments

We thank P. MacLeish (Morehouse School of Medicine), D. Forrest (NIDDK), C. Craft, G. Chader (USC), C. Gregory-Evans, R. Molday (University of British Columbia), P. Hargrave (University of Florida), Y. Imanishi, K. Palczewsk (CWRU), E. Weiss (UNC), A. Swaroop, T. Li (NEI), R. Lee (UCLA), and J. Saari (University of Washington) for antibodies. We thank T. Baumgartner and P. Byrne (MSKCC) for FACS assistance, N. Lampen (MSKCC) for electron microscopy assistance, N. Zhou, T. Patel and J. Wang for technical assistance, S. Puranik and Z. Li for DNA constructs, and J. Aparicio for critical reading of the manuscript. Funding was received from The Gerber Foundation (X.L.X.), The Fund for Ophthalmic Knowledge (D.H.A.), the Research and Development Funds of the MSKCC Department of Pathology (S.C.J.), The Larry & Celia Moh Foundation (D.C.), and NIH grant 1R01CA137124 (D.C.).

References

1. Weinberg RA. The retinoblastoma protein and cell cycle control. Cell. 1995; 81:323–330. [PubMed: 7736585]
2. Cobrinik D. Pocket proteins and cell cycle control. Oncogene. 2005; 24:2796–2809. [PubMed: 15838516]
3. Gordon GM, Du W. Conserved RB functions in development and tumor suppression. Protein Cell. 2011; 2:864–878. [PubMed: 22180086]
4. Viatour P, Sage J. Newly identified aspects of tumor suppression by RB. Dis Model Mech. 2011; 4:581–585. [PubMed: 21878458]
5. Manning AL, Dyson NJ. RB: mitotic implications of a tumour suppressor. Nat Rev Cancer. 2012; 12:220–226. [PubMed: 22318235]
6. Kleinerman RA, et al. Risk of new cancers after radiotherapy in long-term survivors of retinoblastoma: an extended follow-up. J Clin Oncol. 2005; 23:2272–2279. [PubMed: 15800318]
7. Xu XL, et al. Retinoblastoma has properties of a cone precursor tumor and depends upon cone-specific MDM2 signaling. Cell. 2009; 137:1018–1031. [PubMed: 19524506]
8. McEvoy J, et al. Coexpression of normally incompatible developmental pathways in retinoblastoma genesis. Cancer Cell. 2011; 20:260–275. [PubMed: 21840489]
9. Gombos DS. Retinoblastoma in the perinatal and neonatal child. Semin Fetal Neonatal Med. 2012; 17:239–242. [PubMed: 22622484]
10. Cobrinik, D. Learning about retinoblastoma from mouse models that missed. In: Martinez-Murillo, R.; Martinez, A., editors. Animal Models of Brain Tumors. Springer; New York: 2013. p. 141-152.
11. Lakowski J, et al. Effective transplantation of photoreceptor precursor cells selected via cell surface antigen expression. Stem Cells. 2011; 29:1391–1404. [PubMed: 21774040]
12. Shinoe T, et al. Identification of CD44 as a cell surface marker for Muller glia precursor cells. J Neurochem. 2010; 115:1633–1642. [PubMed: 20969572]
13. Hauck SM, et al. Identification of paracrine neuroprotective candidate proteins by a functional assay-driven proteomics approach. Mol Cell Proteomics. 2008; 7:1349–1361. [PubMed: 18436526]
14. Xu XL, et al. Tumor-associated retinal astrocytes promote retinoblastoma cell proliferation through production of IGFBP-5. Am J Pathol. 2010; 177:424–435. [PubMed: 20508032]
15. Wang H, et al. Skp2 is required for survival of aberrantly proliferating Rb1-deficient cells and for tumorigenesis in Rb1+/− mice. Nat Genet. 2010; 42:83–88. [PubMed: 19966802]
16. Lee TC, Almeida D, Claros N, Abramson DH, Cobrinik D. Cell cycle-specific and cell type-specific expression of Rb in the developing human retina. Invest Ophthalmol Vis Sci. 2006; 47:5590–5598. [PubMed: 17122153]
17. Sangwan M, et al. Established and new mouse models reveal E2f1 and Cdk2 dependency of retinoblastoma, and expose effective strategies to block tumor initiation. Oncogene. 2012; 31:5019–5028. [PubMed: 22286767]
18. Priya K, Jada SR, Quah BL, Quah TC, Lai PS. High incidence of allelic loss at 16q12.2 region spanning RBL2/p130 gene in retinoblastoma. Cancer Biol Ther. 2009; 8:714–717. [PubMed: 19252413]

19. Ts'o MO, Zimmerman LE, Fine BS. The nature of retinoblastoma. I. Photoreceptor differentiation: a clinical and histopathologic study. Am J Ophthalmol. 1970; 69:339–349. [PubMed: 4190798]
20. Albert DM, Lahav M, Lesser R, Craft J. Recent observations regarding retinoblastoma. I. Ultrastructure, tissue culture growth, incidence, and animal models. Trans Ophthalmol Soc U K. 1974; 94:909–928. [PubMed: 4534142]
21. Popoff NA, Ellsworth RM. The fine structure of retinoblastoma. In vivo and in vitro observations. Lab Invest. 1971; 25:389–402. [PubMed: 5136988]
22. Kapatai G, et al. Gene expression profiling identifies different sub-types of retinoblastoma. Br J Cancer. 2013; 109:512–525. [PubMed: 23756868]
23. Corson TW, Gallie BL. One hit, two hits, three hits, more? Genomic changes in the development of retinoblastoma. Genes Chromosomes Cancer. 2007; 46:617–634. [PubMed: 17437278]
24. Zhang J, et al. A novel retinoblastoma therapy from genomic and epigenetic analyses. Nature. 2012; 481:329–334. [PubMed: 22237022]
25. Dimaras H, et al. Loss of RB1 induces non-proliferative retinoma; increasing genomic instability correlates with progression to retinoblastoma. Hum Mol Genet. 2008; 17:1363–1372. [PubMed: 18211953]
26. DiCiommo DP, Duckett A, Burcescu I, Bremner R, Gallie BL. Retinoblastoma protein purification and transduction of retina and retinoblastoma cells using improved alphavirus vectors. Invest Ophthalmol Vis Sci. 2004; 45:3320–3329. [PubMed: 15326157]
27. Moffat J, et al. A lentiviral RNAi library for human and mouse genes applied to an arrayed viral high-content screen. Cell. 2006; 124:1283–1298. [PubMed: 16564017]
28. Sarbassov DD, Guertin DA, Ali SM, Sabatini DM. Phosphorylation and regulation of Akt/PKB by the rictor-mTOR complex. Science. 2005; 307:1098–1101. [PubMed: 15718470]
29. Cobrinik D, Francis RO, Abramson DH, Lee TC. Rb induces a proliferative arrest and curtails Brn-2 expression in retinoblastoma cells. Mol Cancer. 2006; 5:72. [PubMed: 17163992]
30. Zufferey R, Nagy D, Mandel RJ, Naldini L, Trono D. Multiply attenuated lentiviral vector achieves efficient gene delivery in vivo. Nat Biotechnol. 1997; 15:871–875. [PubMed: 9306402]
31. Wikler KC, Rakic P, Bhattacharyya N, Macleish PR. Early emergence of photoreceptor mosaicism in the primate retina revealed by a novel cone-specific monoclonal antibody. J Comp Neurol. 1997; 377:500–508. [PubMed: 9007188]
32. Li A, Zhu X, Craft CM. Retinoic acid upregulates cone arrestin expression in retinoblastoma cells through a Cis element in the distal promoter region. Invest Ophthalmol Vis Sci. 2002; 43:1375–1383. [PubMed: 11980849]

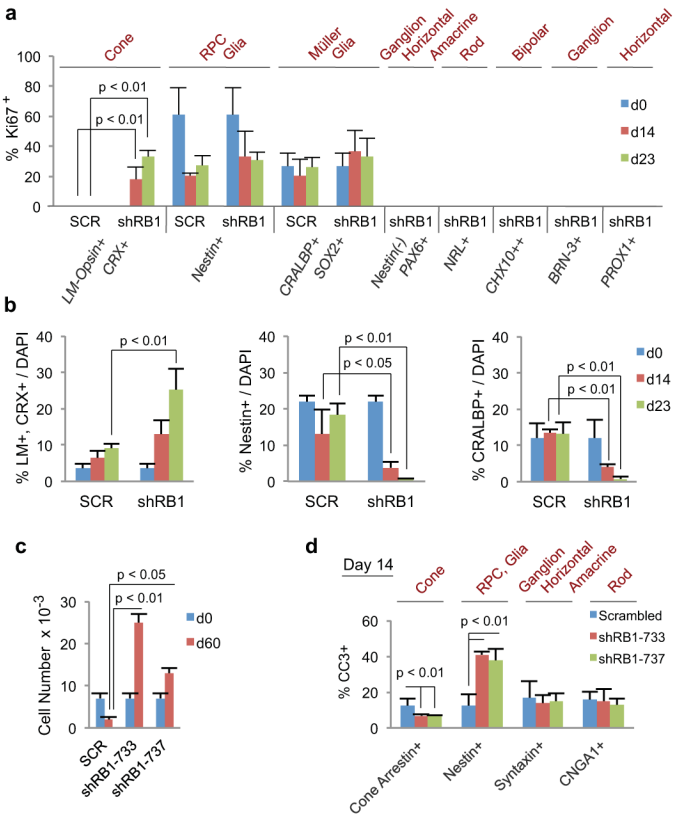

Figure 1. Proliferation of cone-like cells after Rb depletion in dissociated FW19 retina

a–b, Responses to sh*RB1-733*. **a**, Percentage Ki67+ among cells expressing the indicated retinal cell type-specific markers. **b**, Prevalence of DAPI$^+$ cells expressing cone (L/M-opsin, CRX), RPC (nestin), or Müller glia (CRALBP) markers. **c–d**, Responses to sh*RB1-733* and *-737*. **c**, Proliferation of cells, of which >90% were cone marker$^+$ at day 60. **d**, Percentage CC3$^+$ among cells expressing the indicated markers. For all figures, values and error bars represent means plus standard deviations of triplicate assays; P-values are from unpaired Student's t-test. All results replicated at least twice.

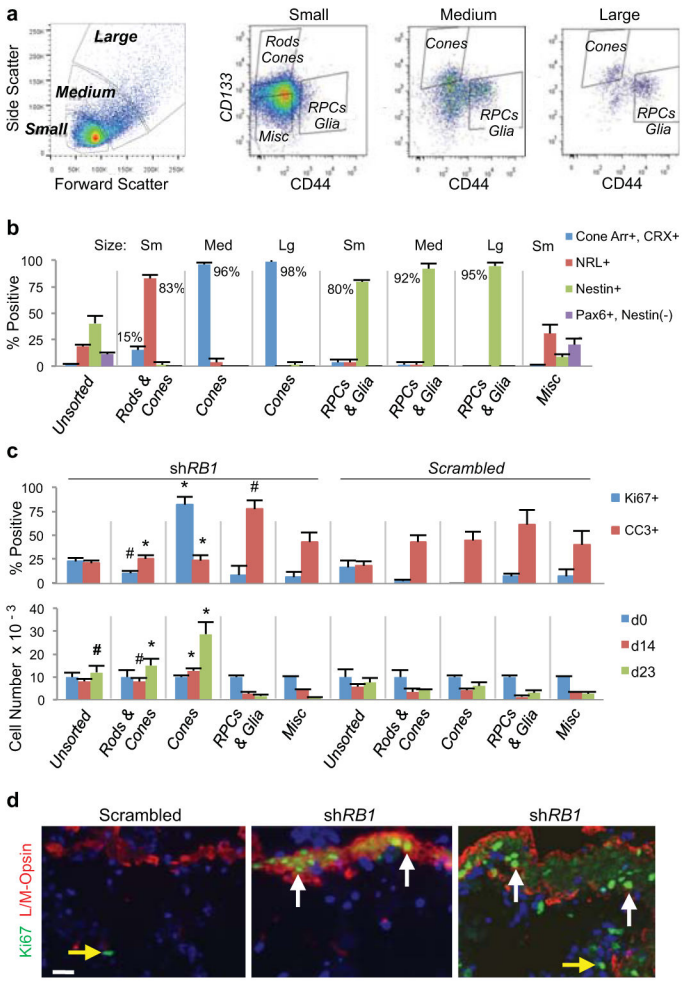

Figure 2. Cone precursor response to Rb depletion

a, FW18 retinal cells sorted by size, CD133, and CD44, with major populations designated. **b**, Percentage of cone arrestin^{+}, CRX^{+} cones, NRL^{+} rods, nestin^{+} RPCs and glia, and PAX6^{+}, nestin$^{(-)}$ horizontal, amacrine, or ganglion cells in each population. **c**, Responses to sh*RB1-733*. Percentage of Ki67^{+} or CC3^{+} cells at 14 days (*top*) and cell numbers at days 14 and 23 (*bottom*). Compared to scrambled control, *****, $p < 0.01$. **#**, $p < 0.05$. Results representative of three independent experiments. **d**, Ki67^{+}, L/M-opsin^{+} cone precursors (white arrows) in FW19 fovea 15 days post-transduction with sh*RB1-733* and *-737*; and Ki67^{+}, L/M-opsin$^{(-)}$ cells likely representing RPCs or glia (yellow arrows) after sh*RB1* or scrambled control. Scale bars, 20 μm.

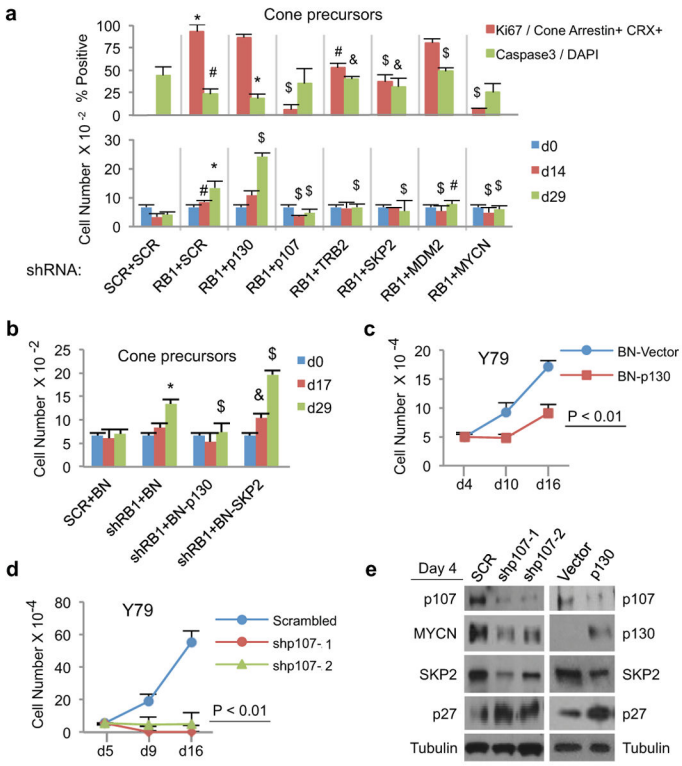

Figure 3. Effects of cone precursor circuitry on response to Rb depletion

a, Prevalence of Ki67^{+} or CC3^{+} cells (*top*) and cell numbers (*bottom*) after shRNA transduction of isolated cone precursors. **b**, Isolated cone precursor response to co-transduction with sh*RB1* and BN vector, BN-*p130*, or BN-*SKP2*. **c–e**, Effect of p130 overexpression or p107 knockdown on Y79 proliferation (**c**, **d**) and protein expression (**e**). Compared to scrambled and vector controls: *, $p < 0.01$. #, $p < 0.05$. Compared to sh*RB1* + SCR (**a**) or to sh*RB1* + BN (**b**): $, $p < 0.01$. &, $p < 0.05$. Results represent at least two independent experiments.

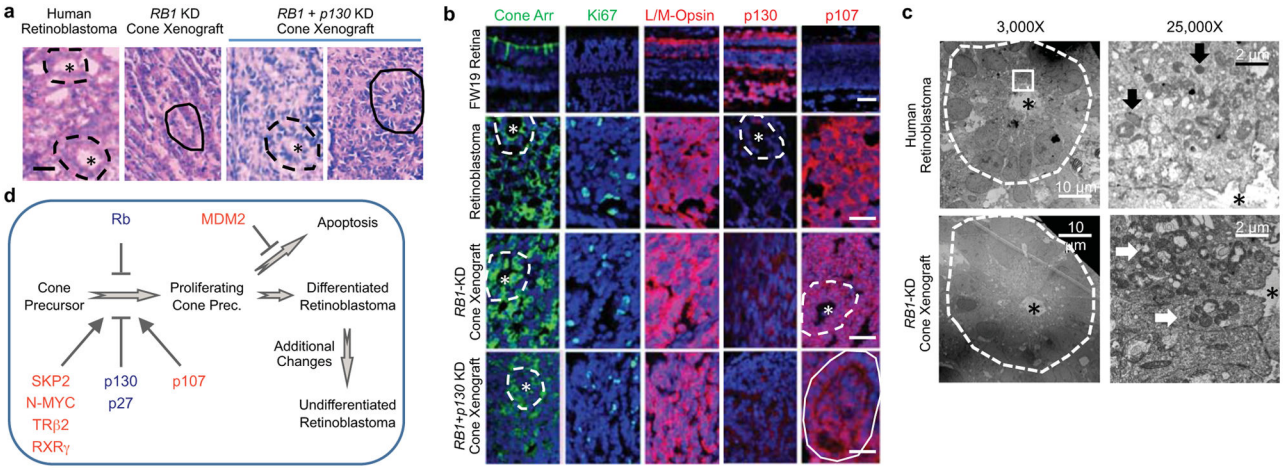

Figure 4. Rb- or Rb/p130-depleted cone precursor tumors

a, Hematoxylin and eosin-stained Rb- and Rb/p130-depleted cone xenograft tumors and human retinoblastoma (n=4). Dashed lines, Flexner-Wintersteiner rosettes. Solid lines, fleurettes. *, rosette cavity. **b**, Cone and cell cycle related protein expression in human retinoblastoma and cone xenografts (n=6). Scale bars, 40 μm (**a**,**b**). **c**, Transmission electron microscopy of Flexner-Wintersteiner rosettes in human retinoblastoma and a cone-derived tumor, with mitochondria (arrows) between nuclei and rosette cavity (n=2). 25,000X image from boxed area (*top*). Results are representative of at least two experiments. **d**, Model of cone-precursor retinoblastoma origin highlighting proteins that suppressed (blue) or promoted (red) the proliferative response.